International Journal of Automotive Technology, Vol. 7, No. 5, pp. 555–564 (2006)

1229-9138/2006/029-05

FRONTAL IMPACT FINITE ELEMENT MODELING TO DEVELOP FRP ENERGY ABSORBING POLE STRUCTURE

A. M. ELMARAKBI[1)*] and K. M. SENNAH[2)]

[1)]Space Structure Laboratory, Tohoku University, 6-6-01 Aramaki-Aza-Aoba, Aoba-ku, Sendai 980-8579, Japan
[2)]Department of Civil Engineering, Ryerson University, 350 Victoria St., Toronto, Ontario, Canada, M5B 2K3

(Received 13 December 2005; Revised 7 June 2006)

ABSTRACT–The aim of this paper is to contribute to the efficient design of traffic light poles involved in vehicle frontal collisions by developing a computer-based, finite-element model capable of capturing the impact characteristics. This is achieved by using the available non-linear dynamic analysis software "LS-DYNA3D", which can accurately predict the dynamic response of both the vehicle and the traffic light pole. The fiber reinforced polymer (FRP) as a new pole's material is proposed in this paper to increase energy absorption capabilities in the case of a traffic pole involved in a vehicle head-on collision. Numerical analyses are conducted to evaluate the effects of key parameters on the response of the pole embedded in soil when impacted by vehicles, including: soil type (clay and sand) and pole material type (FRP and steel). It is demonstrated from the numerical analysis that the FRP pole-soil system has favorable advantages over steel poles, where the FRP pole absorbed vehicle impact energy in a smoother behavior, which leads to smoother acceleration pulse and less deformation of the vehicle than those encountered with steel poles. Also, it was observed that clayey soil brings a slightly more resistance than sandy soil which helps reducing pole movement at ground level. Finally, FRP pole system provides more energy absorbing leading to protection during minor impacts and under service loading, and remain flexible enough to avoid influencing vehicle occupants, thus reducing fatalities and injuries resulting from the crash.

KEY WORDS : Vehicle collision, Enery absorption, Fiber Reinforced Polymer (FRP), Finite element analysis

1. INTRODUCTION

In North America, different types of collisions of vehicles are recorded each year, resulting in thousands of injuries and fatalities. The severity of these collisions depends on the aggressiveness and incompatibility in vehicle-to-vehicle, vehicle-to-pole, vehicle-to-curbs, and vehicle-to-guardrail collisions.

Worldwide statistics show that motor vehicle crashes are the leading cause of death and injury despite improved crashworthiness of vehicles, enhanced road sign, and sophisticated safety systems. In fact, traffic accidents take a half million lives and injure another 15 million occupants around the world each year, and the numbers are growing along with the growth of the world's urban areas, as stated in the Annual World Disasters Report (2003). Transport Canada (2004) reported that 2,936 vehicle occupants were killed and 227,768 were injured in traffic collisions. In the EU countries, transport crashes killed about 39,200 citizens in 2001, caused over 3.3 million injuries and presently cost over 180 billion Euros, around twice the total EU budget for all activity and untold pain and suffering (European Transport Safety Council, 2003). The U.S. National Center for Statistics and Analysis (NCSA, 2002) reported that a total of 42,815 people lost their lives and another 3.0 million people were injured in motor vehicle crashes in 2002. The health and economical burden of these alarming statistics on society is devastating. The National Highway Traffic Safety Administration NHTSA (2003) estimated that highway crashes cost the United States society $230.6 billion a year.

Collisions between vehicles leaving the road and unforgiving roadside objects (trees, poles, and road sign) are a major road safety problem. Such collisions contribute to about 32 percent of the total fatal accidents in the United States, Traffic Safety Facts (NHTSA, 2004), and between 18 and 42 percent in several EU countries, ETSC report (European Transport Safety Council, 1998).

The severity of these collisions with roadside furniture depends partly on the incompatibility of vehicle-to-roadside hardware collisions (Elmarakbi and Zu, 2005). Narrow objects like trees, utility poles and guardrail terminals subject the side of the vehicle to highly

*Corresponding author. e-mail: ahmed.elmarakbi@utoronto.ca

concentrated loads that are difficult to resist without extensive vehicle deformation.

Vehicle crashworthiness focuses on the capability of a vehicle to protect its occupants in the event of a crash. The evaluation of such crashworthiness has involved numerous full-scale crash tests of the vehicle and roadside hardware to verify the compliance with regulatory requirements. Such experimental crash testing is expensive as well as time consuming, particularly at the early stages of developing reference values and improved design criteria. Hence, the need to simulate the crash event by analytical procedure has been an evolving research issue.

Computer simulation tools are increasingly being used for the upfront assessment of crashworthiness without going through multiple-cycles of prototype testing and iterative design changes. In fact, combining real world (forensic, statistical, and crash reconstruction) observations with rigorous modeling and carefully controlled laboratory testing lead to highly effective solutions. As such, they present opportunities for improvements and countermeasure development to prevent recurrence of similar events. Very few researchers have conducted finite-element computer simulation of vehicle collisions to traffic light poles (Wekezer *et al.*, 1993; Ray, 1997; Tabiei and Wu, 2000; and Kirkpatrick *et al.*, 2003).

Street and highway lighting are some of the recent common applications for Fiber Reinforced Polymer (FRP) poles. These poles can be embedded in soil or bolted to a concrete foundation. These poles are environmental friendly and used to replace wooden poles. These poles have been designed and tested for wind and snow loads, with no information on their crashworthiness when impacted by vehicles. Crashworthiness is assessed by means of energy absorbed by the pole, deformation and acceleration.

The objective of this paper is to use the finite element dynamic simulation technique to evaluate vehicle crashworthiness as well as the structural response of traffic light poles made of steel and FRP composite materials, embedded in different soil conditions in frontal vehicle collisions.

2. FINITE ELEMENT MODELING

Initial research on highway vehicle impact simulations began in the mid-1960's. Some computer codes resulted from that early work. However, these programs were not easy to use and because of computer hardware limitations of that period, many simplifying assumptions were required in order to utilize them economically in the analysis. For example, the number of elements that could be used in a model was very limited, the vehicle was represented as lumped masses, and the interactions between the impacting structures were very approximate in form. Minor modeling adjustment and maintenance continued till mid-1980's. Since then, there have been extensive advances in the finite-element method primarily due to the availability of increased computational power and large funding levels to military, aerospace and automotive industries. Of the commercially available finite-element software, LS-DYNA3D (Livermore Software Technology Corporation, 2002) developed by Livermore Software Technology Corporation of California, is capable of performing finite-element impact analysis using explicit, geometric and material nonlinear codes for dynamic response.

2.1. Vehicle Model

In this paper, a finite-element (FE) model for a midsize sedan vehicle as shown in Figure 1 was ultilized in this study.

This vehicle model is based on a 1991 Ford Taurus 4-door (FHWA/NHTSA, 2002). The major characteristics of the complete FE vehicle model can be identified as follows: (1) 28182 shell elements, 303 beam elements and 349 solid elements; (2) 141 material cards, defining the material models employed, including steel, rubber, honeycomb, and glass; (3) Rigid (stone) wall for representing the ground; (4) automatic single surface contact from A-pillar to bumper; (5) tied nodes to surface contact between the column and the plate; (6) automatic nodes to surface contact between the bumper and the column; (7) conventional, spot weld, and rigid body nodal constraints; and (8) discrete springs, and discrete masses. The front-end components from bumper to A-pillar are modeled with a fine mesh, while the rear half of the vehicle had a fairly coarse mesh density. Components like bumper, front rails, upper load path beams, radiator, engine cradle, etc., are modeled to capture all significant geometric imperfections such as holes, beads and crush initiators that play a vital role in overall crash characteristics of a vehicle.

2.2. Traffic Light Pole Model

Two different pole materials are used in this paper,

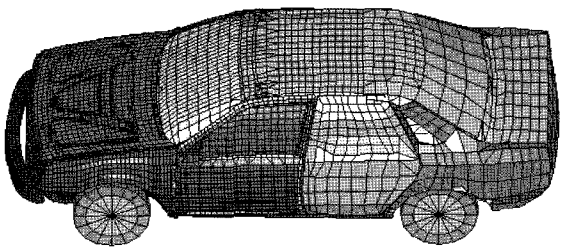

Figure 1. Schematic view of finite element model of the vehicle.

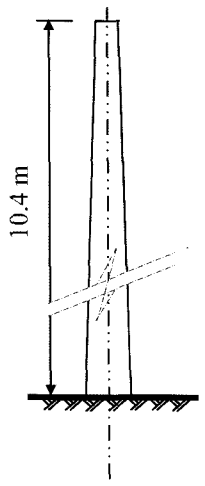

Figure 2. Steel pole.

namely: steel and FRP for a typical pole shown in Figure 2.

In this paper, the pole is considered embedded directly into the soil to a certain depth. The poles are of round cross section with bottom diameter of 0.334 m, top diameter of 0.133 m, and height above ground level of 10.40 m. The Pole is embedded into the soil at a depth of 1.80 m and impacted by a vehicle in frontal situation with 32 km/hr impact speed.

The pole is modeled using shell elements to capture the three-dimensional effects of the structure. Due to its computational efficiency, the Belytschko-Lin-Tsay formulation is chosen for this simulation. Such a shell element is based on a combined co-rotational and velocity strain formulation.

The FE model consisted of 824 shell elements above the ground level and 144 shell elements (18 elements in the vertical direction × 8 elements in the lateral direction) in the pole's part under the ground for a depth of 1.8 m. The wall thickness of the pole was taken as 3 mm. Steel pole materials are considered with following mechanical properties (ASTM, 1990):

Density ρ=7830 kg/m^3, Young's modulus E=207 GPa, Yield stress σ_y=215 MPa, Poisson's ratio υ= 0.28.

Table 1. Effective plastic strain and corresponding yield stress of steel material.

Effective plastic strain values	Corresponding yield stress values (MPa)
0.0	215
0.004	300
0.03	390
0.15	440
0.30	460
0.40	400

The steel pole is modeled using an elasto-plastic material (material type 24 in LS-DYNA3D user's manual) with an arbitrary stress versus strain curve with values given in Table 1. The key card for material type 24 is defined as (MAT_PIECEWISE_LINEAR_ PLASTICITY).

In addition, the FRP pole is fabricated using type-E fiberglass and vinyl ester resin with a target glass/resin ratio of 70/30% by weight. The material coordinate system of the FRP pole is defied as: Material set of axes (1, 2 and 3); axes 1 and 2 are tangent to the surface, while axis 3 is perpendicular to the surface of the shell. Axis 1 is directed along the fiber direction. The mechanical properties along the 1–2 directions (1 is the fibers direction and 2 is an axis perpendicular to the fibers in the plane of the plate) are given as following (Mikhail and El Damatty, 1999).

Density ρ=1820 kg/m^3, E_1=36.85 GPa, E_2=11.16 GPa, G_{12}=G_{13}=3.36 GPa, G_{23}=4.32 GPa, υ_{12}=υ_1=υ_{12}=0.3, σ_T^{U1} = 552.775 MPa, σ_C^{U1} =442.22 MPa, σ_T^{U2} =16.74 MPa, σ_C^{U2} =89.25 MPa, τ^U=70.57 MPa

where σ^U is the ultimate stress of the material; the superscripts 1 and 2 correspond to material axes 1 and 2, respectively; the subscripts T and C correspond to tensile and compression ultimate stresses, respectively; τ^U is the ultimate shear stress; υ is the Poisson's ratio; E is the modulus of elasticity and G is the shear modulus. The FRP pole is modeled using material type 59 in LS-DYNA3D user's manual. The key card for material type 59 is defined as (MAT_COMPOSITE_FAILURE_ SHELL_MODEL).

3. SOIL-POLE INTERACTION MODELING

Two different soil materials were considered in this study, namely: clayey and sandy soils. The following subsections explain the methodology used to model soil-pole interaction.

Shell elements were used to model the embedded part of the pole. Modelling the soil using spring elements have been used and validated by many researchers (Tabiei and Wu, 2000; Plaxico *et al.*, 1998, 1999; Matej and Zoran, 2004). Eight springs representing the lateral resistance of the soil are identified in the horizontal direction at each node levels of the embedded part to cover all possible vehicle impact scenarios. Also, the friction resistance of the soil is represented by eight springs in the vertical direction at each node levels of the embedded part as shown in Figure 3.

Since pole separation is possible under lateral loads, spring elements are identified to carry compressive forces only. As in the direction of impact shown in Figure 3 only three springs (1, 2 and 3) are loaded (compression load). The other springs in this case don't actually carry any loads (tension load). Since three springs are considered in

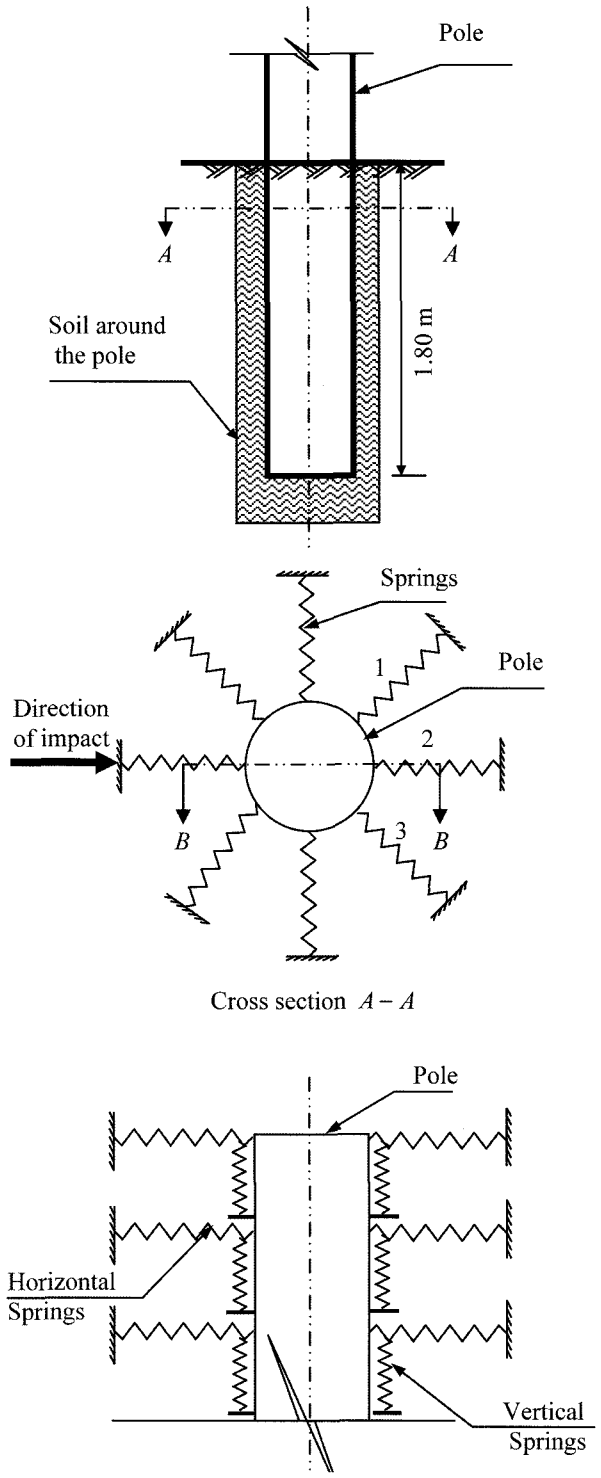

Figure 3. Pole embedded into soil.

each direction of impact, the response of a single response is divided by three springs (Plaxico *et al.*, 1998, 1999). Similarly, if a vehicle collides the pole from any direction, only three springs are loaded and analyzed.

The following subsections summarize the equations from which the spring constants were obtained (Mosher and Dawkins, 2000).

3.1. Lateral Resistance for Clay

A series of lateral load tests on instrumented piles in clay (Matlock, 1970) were used to produce the force-displacement (*p-u*) relationship for piles in soft to medium clays subjected to static lateral loads in the form of:

$$P=0.5P_u \cdot (y/y_c)^{1/3} \tag{1}$$

where P is the actual lateral resistance of soil, y is the actual lateral displacement and P_u is the ultimate lateral resistance, given by the smaller of

$$P_u=\left(3+\frac{\gamma'}{c}\cdot x+\frac{J}{D}\cdot x\right)\cdot c\cdot D,\quad x<x_{cr} \tag{2}$$

for a wedge failure near the ground surface, and

$$P_u=9\cdot c\cdot D,\quad x\geq x_{cr} \tag{3}$$

for flow failure at a certain depth; and y_c is the lateral displacement at one-half of the ultimate resistance, given by

$$y_c=2.5\varepsilon_c\cdot D \tag{4}$$

where γ' is the effective unit weight of clayey soil=961 kg/m^3, c is the shear strength of the soil=34.5 kN/m^2, J is dimensionless empirical constant=0.25 for medium clay, ε_c is the strain at 50 percent of the ultimate strength from a laboratory stress- strain curve=0.01, D is the pole diameter and x is the depth below ground surface.

The depth at which failure transitions from wedge, Equation (2), to flow type, Equation (3), is

$$x_{cr}=\frac{6\cdot c\cdot D}{\gamma'\cdot D+J\cdot c} \tag{5}$$

Figure 4 shows the force-deformation characteristics of the horizontal springs at different soil depths of clayey soil.

3.2. Lateral Resistance for Sand

The ultimate lateral resistance for sand was found to vary from a value at shallow depths, P_{us}, determined by Equation (6) to a value at deep depths, P_{uD}, determined by Equation (7). At a given depth the equation giving the smallest value of P_u should be used as the ultimate lateral resistance.

$$P_{us}=(C_1\cdot x+C_2\cdot D)\cdot\gamma'\cdot x \tag{6}$$

$$P_{uD}=C_3\cdot D\cdot\gamma'\cdot x \tag{7}$$

where γ' is the effective unit weight of sandy soil = 1040 kg/m^3, C_1, C_2 and C_3 are coefficients as a function of ϕ and equal 3, 3.5, and 54, respectively, and ϕ is angle of

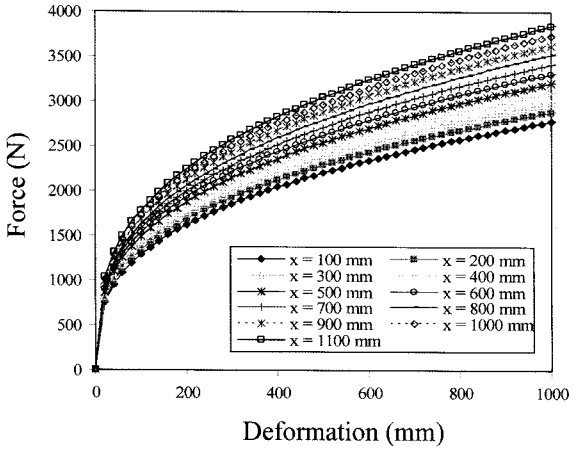

(a) Embedment length of 100 to 1100mm

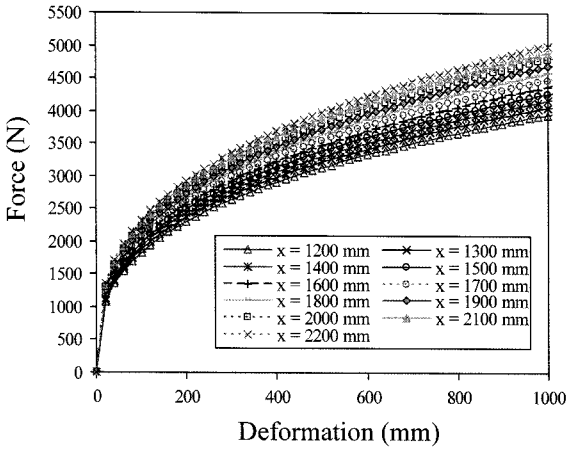

(b) Embedment length of 1200 to 2200 mm

Figure 4. Force–deformation characteristics of the horizontal springs at different depths in clayey soil.

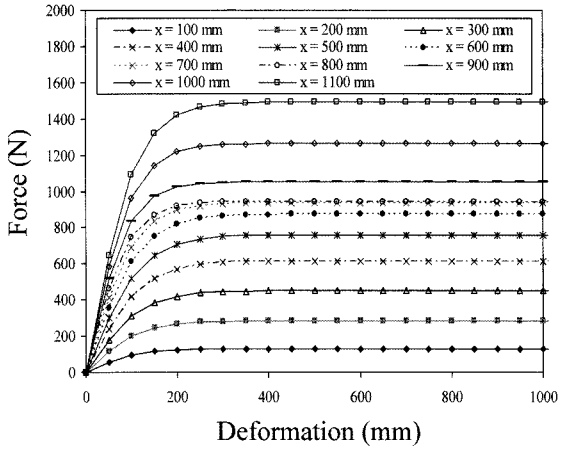

(a) Embedment length of 100 to 1100mm

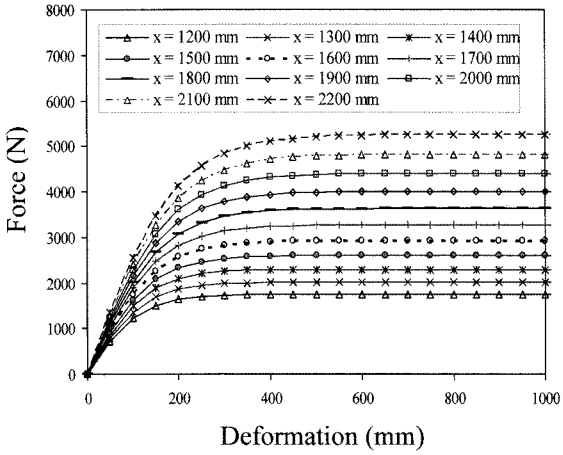

(b) Embedment length of 1200 to 2200 mm

Figure 5. Force–deformation characteristics of the horizontal springs at different depths in sandy soil.

internal friction of sand=35°.

The force-deformation relationship for sand is also nonlinear and in the absence of more definitive information for cyclic loading, the following expression is used by Murchison and O'Neill (1984) for lateral resistance at depth x:

$$P=n \cdot A \cdot P_u \cdot \tanh\left(\frac{k \cdot x \cdot y}{n \cdot A \cdot P_u}\right) \quad (8)$$

where P_u is the ultimate lateral soil resistance from either Equation (6) for $x < x_{cr}$ or Equation (7) for $x \geq x_{cr}$, k is the initial modulus of subgrade reaction=21,720 kN/m^3, n is a geometry factor=1, and A is calculated as follows:

$$A=3-0.8\left(\frac{x}{D}\right) \geq 0.9 \quad (9)$$

Figure 5 shows the force-deformation characteristics of the horizontal springs at different depths of sandy soil. In this study, the characteristics values of vertical springs are considered 10% of the horizontal values (Ferritto *et al.*, 1999).

4. SIMULATION RESULTS

4.1. Influence of Soil and Pole Material Type

In this section, the effects of soil and pole material types are addressed. Four cases are studied to capture the dynamic response of the vehicle/pole impact, namely: (i) steel pole embedded into clayey soil; (ii) steel pole embedded into sandy soil; (iii) FRP pole embedded into clayey soil; and (iv) FRP pole embedded into sandy soil. The vehicle model is given an initial velocity of 32 km/hr to impact the pole in frontal impact scenario.

Nonlinear finite element dynamic simulation using LS-DYNA3D is performed for the first 1000 ms time period of the vehicle impacting the pole. The average

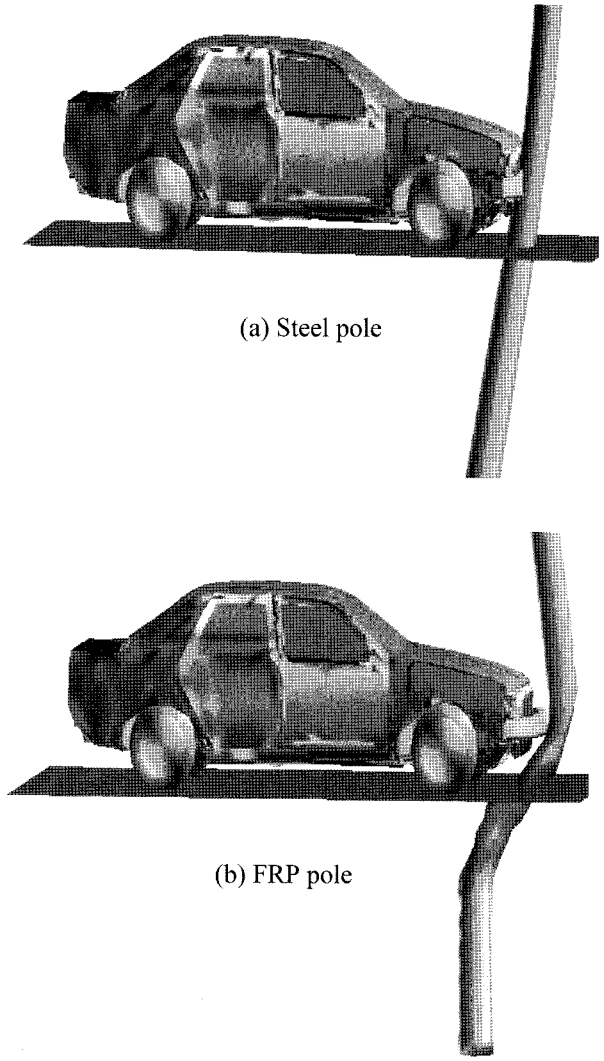

(a) Steel pole

(b) FRP pole

Figure 6. Vehicle impact to the pole embedded into soil.

CPU time varied from 82 to 86 hours for each run. Figure 6 shows the deformation of both the vehicle and the pole at 100 ms.

Initial contact between the vehicle and the pole occurred at 0.0 msec. Immediately after impact, the pole began to deform and to displace laterally in the soil. It is shown that the steel pole has less deformation characteristics compared to the FRP pole. Therefore, deformation of the vehicle's front-end is minimized when involved with FRP compared to large deformation of the vehicle's front-end in the case of steel pole impact.

It is worth to mention that the FRP composite energy absorbing poles are not designed to break away. It is also shown that the impact energy is absorbed via an excessive damage in the FRP pole compared to steel pole as shown in Figure 7. The damage behavior of the FRP pole is in good agreements with the composite pole

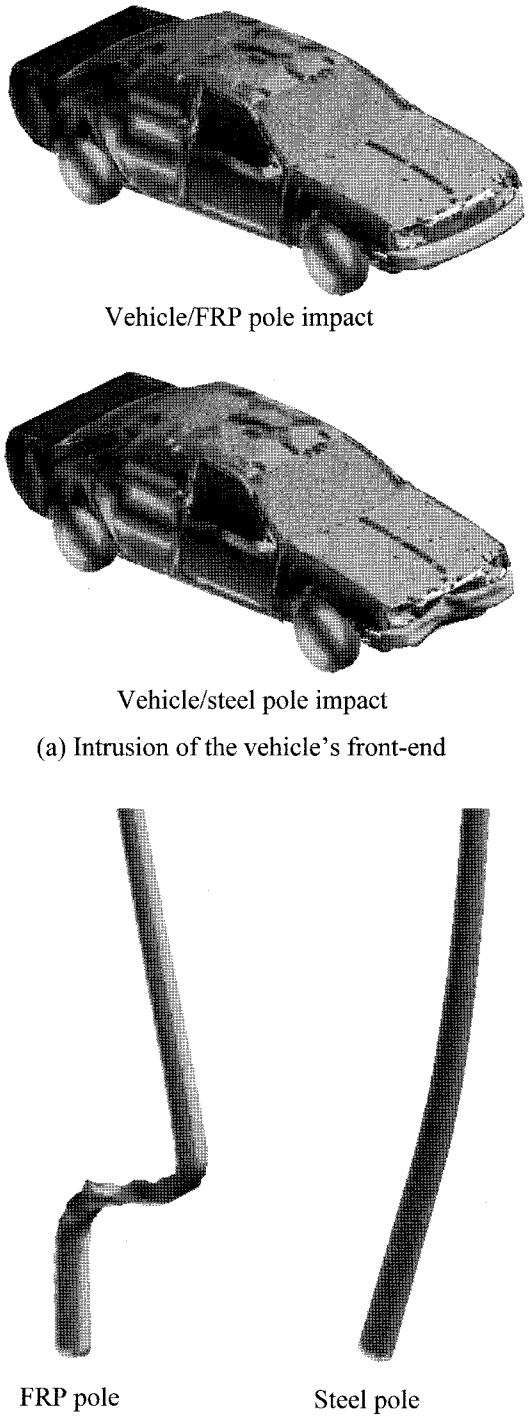

Vehicle/FRP pole impact

Vehicle/steel pole impact

(a) Intrusion of the vehicle's front-end

FRP pole Steel pole

(b) Damage of the pole

Figure 7. Intrusion of the vehicle's front-end and damage in the pole.

damage results obtained by Foedinger *et al.* (2003). In their work, they used high speed impact, however, the damage behavior are the same.

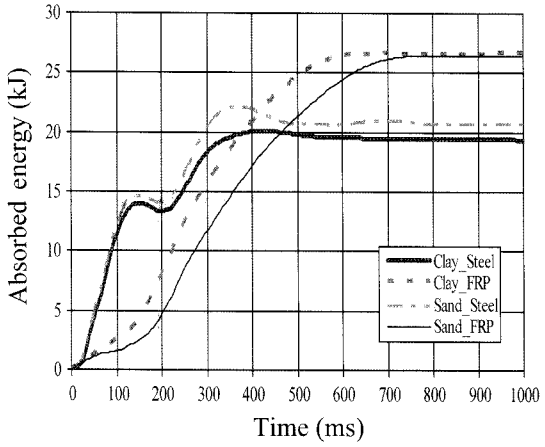

Figure 8. Energy absorbed by the pole-soil system in case of FRP and steel poles embedded in clayey and sandy soils for 32 km/hr impact velocity.

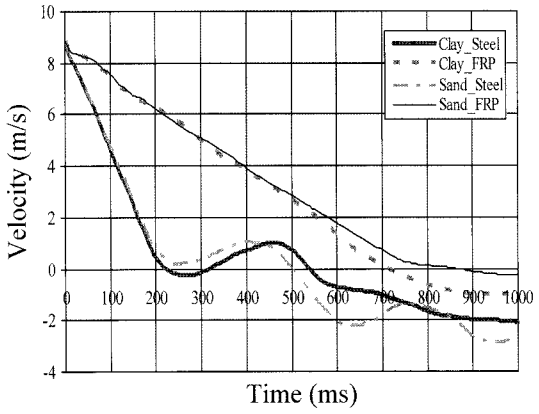

Figure 9. Velocity of the passenger compartment in case of FRP and steel poles embedded in clayey and sandy soils for 32 km/hr impact velocity.

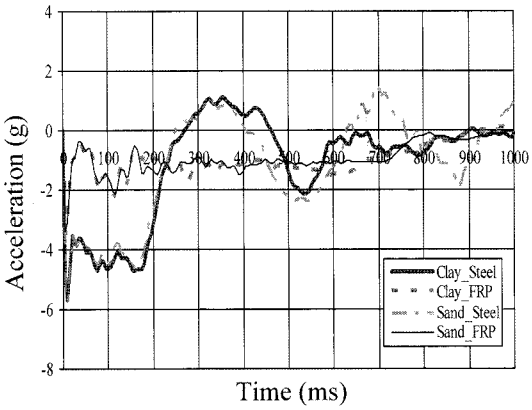

Figure 10. Acceleration of the passenger compartment in case of FRP and steel poles embedded in clayey and sandy soils for 32 km/hr impact velocity.

Figure 8 shows the amount of energy absorbed by the pole at 32 km/hr impact speed. It can be observed that the steel pole embedded into clayey and sandy soil absorbed a maximum of 20 and 22 kJ, respectively, at about 400 ms. Then, no more energy absorbed till reaching 1000 ms. However, the FRP pole embedded into clayey and sandy soil absorbed a maximum of 26.6 and 26.4 kJ, respectively, at about 700 ms. This may be attributed to the high deformation occurred in the FRP pole as a result of the impact. It is worthnoting that there is a slight improvement in energy absorption capabilities in case of clayey soil compared to sandy soil in case of FRP pole, while there is a slight improvement in energy absorption capabilities in case of sandy soil compared to clayey soil in case of steel pole.

These results indicate that the steel pole exhibits more resistance to the impact than the FRP pole at 32 km/hr impact speed. Since the FRP pole embedded in clayey and sandy soil demonstrated high energy absorption capabilities at 32 km/hr impact speed, the deformation of the vehicle's front-end is considerably less than that for steel pole as also shown in Figure 7.

The time histories of velocities of the passenger compartment are depicted in Figure 9. It is shown that the steel pole stopped the vehicle after about 225 ms from the initiation of the impact, while the FRP pole required about 800 ms to stop the vehicle. This behavior illustrates the smoothness of performance of the FRP pole when involved in vehicle collision; it took longer time to stop the vehicle and to transfer all kinetic energy to internal energy.

The time histories of the accelerations of the passenger compartment are given in Figure 10 at 32 km/hr impact speed for both steel and FRP poles. It is shown that the vehicle suffers a high acceleration pulse in case of steel pole embedded into sandy and clayey soils, about 5.7 g, due to the high resistance of the steel pole to the impact, while it suffers lower acceleration in case of FRP pole embedded into sandy and clayey soils, about 3.5 g, with longer crash time zone due to the flexibility of the FRP pole.

In addition, the movement of the pole at the point of impact is depicted in Figure 11.

It is noticed that the steel pole embedded into sandy and clayey soils displaced less distance, about 0.7 m, than the FRP pole embedded into clayey and sandy soils that displaced about 3.0 m. It is also shown that the FRP pole reaches maximum displacement at about 700 ms and in the case of sandy soil, however, it retracts after 700 ms in the case of the clayey soil. On the other hand, the steel pole reached the maximum displacement at about 550 ms and then retracts irrespective of soil type. This behavior confirms the impact smoothness for FRP pole when

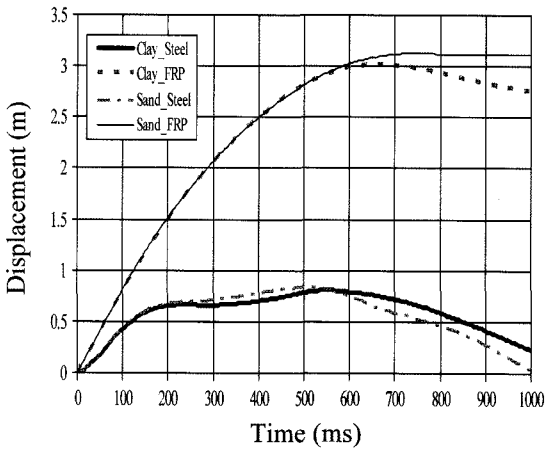

Figure 11. Movement of the pole at the point of impact in case of FRP and steel poles embedded in clayey and sandy soils for 32 km/hr impact velocity.

involved in frontal collision. This leads to better protection during impacts and to remain flexible enough to avoid influencing vehicle occupants, thus reducing fatalities and injuries resulting from the crash.

4.2. Influence of Impact Velocity

In impact simulation of FRP pole system, the vehicle model is given three different initial velocities, 16, 24 and 32 km/hr, respectively, to collide the pole in frontal impact scenario. Figures 12 to 15 show the effects of impact speed on the dynamic response of the vehicle and the FRP pole embedded in clayey soil.

It is clear from Figure 12 that the absorbed energy by the FRP pole-soil system increases with increase in the impact speed. For example, at 32 km/hr speed impact, the pole absorbed 26.6 kJ compared to 3.7 kJ at impact speed of 16 km/hr.

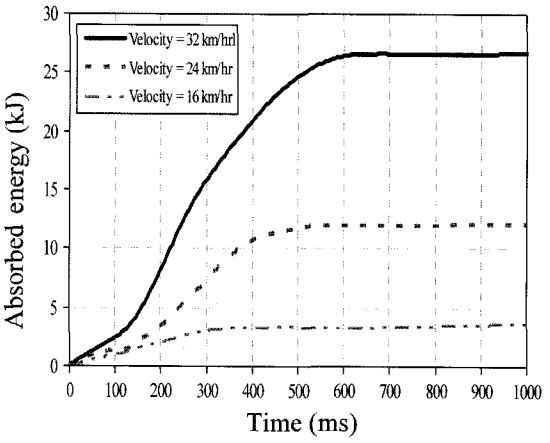

Figure 12. Energy absorbed by the pole-soil system in case of FRP poles embedded in clayey soil at different impact velocities.

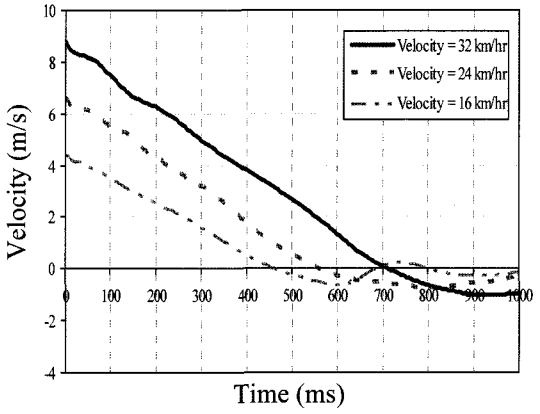

Figure 13. Velocity of the passenger compartment in case of FRP poles embedded in clayey soil at different impact velocities.

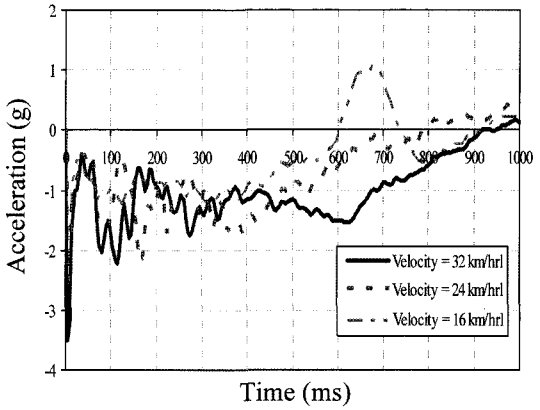

Figure 14. Acceleration of the passenger compartment in case of FRP poles embedded in clayey soil at different impact velocities.

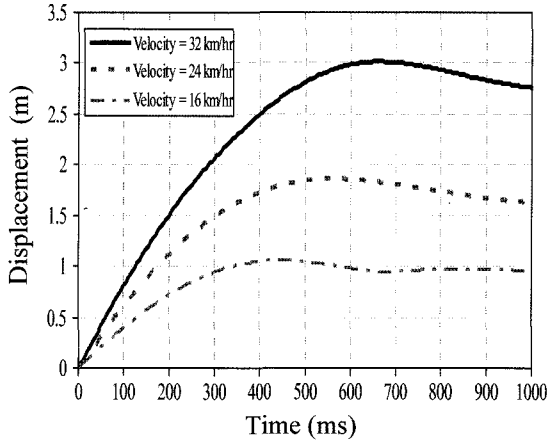

Figure 15. Movement of the pole at the point of impact in case of FRP poles embedded in clayey soil at different impact velocities.

Different velocity profiles of the passenger compartment are depicted in Figure 13, which shows that the FRP pole stopped the vehicle after about 720 ms at 32 km/hr impact speed and after about 470 ms at 16 km/hr impact speed.

It is clear from Figure 14 that the acceleration of the vehicle's passenger compartment increases with increase in the impact speed. It is shown that, at high speed impacts such as 32 km/hr, the peak value of the acceleration pulse reached about 3.5 g compared to about 1.8 g at 16 km/hr impact speed. The movements of the pole at the point of impact during collision are shown in Figure 15. It is noticed that the pole displaced 3.0 m at 32 km/h impact speed while it displaced 1.05 m at 16 km/hr impact speed and then stopped the vehicle.

5. CONCLUSIONS

The results of this study on the performance steel and FRP traffic light poles in vehicle crash accidents support the following findings:

(1) the type of pole material has a significant effect on the energy absorption characteristics of the system. The more flexible the pole material is, the more the energy absorbed by the pole and the less the intrusion of the vehicle into the vehicle compartment. This may have a considerable input as a life-saving and/or injury-reducing factor for vehicle occupants in the event of a crash. It is worthynoting that the FRP pole does not break away and stops the vehicle gently. Moreover, the FRP pole absorbs vehicle impact energy in a smoother manner, which leads to smoother acceleration pulse and less deformation of the vehicle than those encountered with steel poles.

(2) clayey soil brings a slightly more resistance than sandy soil, which reduces pole movement at the ground level.

ACKNOWLEDGEMENT–The authors wish to acknowledge the financial support provided by canadian networks of centers of excellence of the automobile of 21st century (nce-auto21).

REFERENCES

ASTM Int. (1990). *Metals Handbook.* **2**- Properties and selection: nonferrous alloys and special purpose materials. 10th Edn, Ohio, USA.

Elmarakbi, A. and Zu, J. (2005). Crashworthiness improvement of vehicle-to-rigid fixed barrier in full frontal impact using novel vehicle's front-end structures. *Int. J. Automotive Technology* **6, 5,** 491–499.

European Transport Safety Council (1998). *Forgiving Roadsides.* Brussels, Belguim.

European Transport Safety Council. (2003). *Transport Safety Performance in the EU: A Statistical Overview,* Brussels, Belguim.

Ferritto, J., Dickenson, S., Priestley, N. and Taylor, C. (1999). *Seismic Criteria for California Marine Oil Terminals, Chapter 3: Structural Criteria for Piers and Wharves.* NFESC Technical Report TR 2103-SHR, 26-38, CA, USA.

FHWA/NHTSA (2002). http://www.ncac.gwu.edu/archives/model/. *National Crash Analysis Center George Washington University,* U.S.A.

Foedinger, R., Boozer, J., Bronstad, M. and Davidson, J. (2003). Development of energy-absorbing composite utility pole. *Transportation Research Record No. 1851, Highway and Facility Design,* 149–157.

Int. Federation of Red Cross and Red Crescent Societies (2003). *The Annual World Disasters Report.* New York, USA.

Kirkpatrick, S., MacNeill, R. and Bocchieri, R. (2003). Development of an LS-DYNA occupant model for use in crash analyses of roadside safety features. Transportation Review Board, Paper No. TRB2003-0002450, *Proc. 2003 TRB 82nd Annual Meeting,* Washington D.C., USA, CD-ROM, 1–15.

LS-DYNA User's Manual (2002). Livermore Software Technology Corporation. California, U.S.A.

Matej, V. and Zoran, R. (2004). Reducing the vehicle impact severity with improved road restraint system. *FISITA 2004 World Automotive Congress,* Barcelona, Spain, CD ROM, 1–8.

Matlock, H. (1970). Correlations for design of laterally loaded piles in soft clay. *2nd Annual Offshore Technology Conf., Paper No. 1204,* **1,** 577–588.

Mikhail, A. and El Damatty, A. (1999). Non-linear analysis of FRP chimneys under thermal and wind loads. *Thin-Walled Structures,* **35,** 289–309.

Mosher, R. and Dawkins, W. (2000). Theoretical manual for pile foundations. *US Army Corps of Engineers,* USA, 32–42.

Murchison, J. and O'Neill, M. (1984). Evaluation of p-y relationships in cohesionless soils. Analysis and design of pile foundations, *American Society of Civil Engineers,* 174–191.

National Center for Statistics and Analysis (NCSA). (2002). *Fatalities and Injuries to 0-8 Year Old Passenger Vehicle Occupants based on Impact Attributes.* DOT HS 809 410, Washington D.C., USA.

National Center for Statistics and Analysis (NCSA). (2002). *Traffic Safety Facts 2000.* DOT HS 809 324, Washington D.C., USA.

NHTSA (2003). *DOT Releases Preliminary Estimates of 2002 Highway Fatalities.* News Release, NHTSA 13-03, Washington D.C., USA.

NHTSA (2004). *Traffic Safety Fcts 2002: A Compilation*

of Motor Vehicle Crash Data from the Fatality Analysis Reporting System and the General Etimates System. DOT HS 809 620, Washington D.C., USA.

Plaxico, C., Patzner, G. and Ray, M. (1998). Finite element modeling of a guardrail post mounted in soil. *12th Engineering Mechanics Conf.*, ASCE, NY, USA, 1–4.

Plaxico, C., Patzner, G., and Ray, M. (1999). Finite element modeling of guardrail timber posts and the post-soil interaction. *Transportation Research Record*, Paper No. 980791, Washington D.C., 1–24.

Ray, M. (1997). The use of finite element analysis in roadside hardware design; *Int. J. Crashworthiness*, **2,** 333–348.

Tabiei, A., and Wu, J. (2000). Roadmap for crashworthiness finite element simulation of roadside safety structures. *Finite Elements in Analysis and Design*, **34,** 145–157.

Transport Canada (2004). *Canadian Motor Vehicle Traffic Collision Statistics.* TP 3322.

Wekezer, J., Oskard, M., Logan, R. and Zywicz, E. (1993). Vehicle impact simulation. *ASCE J. Transportation Engineering*, **199,** 598–617.